J Appl Electrochem (2007) 37:1287–1302
DOI 10.1007/s10800-007-9418-x

ORIGINAL PAPER

Effects of non-linear kinetics on free convection in an electrochemical cell with a porous separator

K. I. Borg · K. E. Birgersson · F. H. Bark

Received: 7 March 2007 / Revised: 6 September 2007 / Accepted: 6 September 2007 / Published online: 5 October 2007
© Springer Science+Business Media B.V. 2007

Abstract The spatial evolution of the ionic concentration of an electrolyte in an isothermal electrochemical cell with a porous separator between the electrodes was investigated for large values of Rayleigh number. The reaction kinetics were described by the Butler–Volmer equation. The full problem, involving the coupled partial differential equations describing the velocity field, the ionic concentration, and the electric potential, was reduced by means of regular and singular perturbation theory, to a simplified evolution equation, coupled with a transcendental function for the ionic concentration and electric potential; the solution was found to agree well with the numerical solution of the full problem. In the limit of large and small cell voltages, closed analytical solutions were secured for the concentration, potential, and overall current density.

Keywords Natural convection · Reaction kinetics · Porous separator

K. I. Borg (✉)
Department of Mechanical Engineering and Science, Graduate School of Engineering, Kyoto University, Kyoto 606-8501, Japan
e-mail: kborg@mech.kth.se

Present Address:
K. I. Borg
Norra Real, Roslagsgatan 1, SE-113 55 Stockholm, Sweden
e-mail: kalle.borg@gmail.com

K. E. Birgersson
Engineering Science Programme, Department of Chemical and Biomolecular Engineering, National University of Singapore, Singapore 117576, Singapore
e-mail: chebke@nus.edu.sg

F. H. Bark
Department of Mechanics, Royal Institute of Technology, Stockholm 100 44, Sweden
e-mail: fritz@mech.kth.se

Nomenclature

A	Constant of integration
B	Constant of integration
C_0, C_1	Expansion coefficient of dimensionless concentration
$\mathcal{C}$	Dimensionless concentration
$c^{(i)}$	Concentration of species i, mol m^{-3}
$c_0^{(i)}$	Initial concentration of species i, mol m^{-3}
c	Weighted concentration, mol m^{-3}
c	Dimensionless weighted concentration
$D^{(i)}$	Diffusion coefficient of species i, m^2 s^{-1}
D	Weighted average diffusion coefficient, m^2 s^{-1}
$\boldsymbol{e}$	Unit vector
F	Faraday number, A s mol^{-1}
$\boldsymbol{g}$	Gravitational constant, m s^{-2}
h	Half width of free electrolyte region, m
H	Half height of free electrolyte region, m
$\mathcal{H}$	Dimensionless half height
$\boldsymbol{i}$	Electric current density, A m^{-2}
$\boldsymbol{i}$	Dimensionless electric current density
$\mathcal{I}$	Dimensionless polarization curve
k	Permeability of separator, m^2
$\mathcal{L}$	Dimensionless reduced half height
$\tilde{\mathcal{L}}$	Modified dimensionless reduced half height
$\boldsymbol{N}^{(i)}$	Flux of species i, mol m^{-2} s^{-1}
$\boldsymbol{N}^{(i)}$	Dimensionless flux of species i
$\boldsymbol{N}$	Fictious dimensionless flux
p	Pressure of electrolyte, Pa
p	Dimensionless pressure of electrolyte
r	Dimensionless thickness of vertical boundary layers
Ra	Rayleigh number
$\mathcal{S}'$	Dimensionless stratification

T	Temperature of electrolyte, K
t	Time, s
t	Dimensionless time
V_1, V_2	Potential at electrodes, V
$\mathcal{V}$	Dimensionless potential difference
$\mathcal{V}_{\max}$	Limit value of dimensionless potential difference
$\boldsymbol{v}$	Velocity of electrolyte, m s^{-1}
$\boldsymbol{v}$	Dimensionless velocity of electrolyte
w	Dimensionless vertical velocity of electrolyte
$w_{\pm}$	Dimensionless vertical velocity of electrolyte
x	Horizontal coordinate, m
x	Dimensionless horizontal coordinate
y	Horizontal coordinate, m
z	Vertical coordinate, m
z	Dimensionless vertical coordinate
$\alpha^{(i)}$	Densification coefficient of species i, m^3 mol^{-1}
β	Dimensionless growth velocity of concentration
γ	Transfer coefficient
Γ	Dimensionless number
δ	Dimensionless horizontal boundary layer thickness
ϵ	Perturbation parameter
ζ	Dimensionless slow vertical coordinate
$\tilde{\zeta}$	Modified dimensionless slow vertical coordinate
$\tilde{\zeta}_0$	Constant of integration
$\eta_{\pm}$	Dimensionless stretched coordinates
ϑ	Dimensionless concentration
$\vartheta_{\pm}$	Dimensionless concentration
κ	Dimensionless number
$\lambda_{\pm}$	Dimensionless concentration gradient at electrodes
μ	Kinematic viscosity, m^2 s^{-1}
ν	Dynamic viscosity, kg m^{-1} s^{-1}
Π	Dimensionless reduced pressure
σ	Dimensionless number
τ	Dimensionless slow time
$\Phi_k, k = 0, \ldots, 3$	Auxiliary functions
φ	Porosity of separator
ϕ	Electric potential in electrolyte, V
ϕ	Dimensionless electric potential in electrolyte
ϕ_0, ϕ_1	Expansion coefficients in dimensionless electric potential
ψ_0, ψ_1	Expansion coefficients in dimensionless electric potential
$\mathfrak{k}_1, \mathfrak{k}_2, \mathfrak{k}_3$	Dimensionless constants

1 Introduction

The performance of most electrochemical systems depends on mass transport rates, usually in the form of mass transfer of the participating species to the electrode surfaces. The subsequent electrochemical reactions on the electrode surface can be strongly influenced by the magnitude of the overall mass transport to and from the surface. The modes of mass transport in these systems are migration, diffusion, and convection. Whereas forced convection can easily be controlled, e.g., via pump-induced flow, free convection depends on temperature and concentration gradients in systems, such as metal electrorefining, electroplating, and batteries.

Several studies [1–8] have been carried out to elucidate the main underlying features of free convection in various electrochemical systems. A review is given in [9]. Bark and Alavyoon [3] studied free convection arising during unsteady electrolysis of a dilute solution with a metal salt and vertical electrodes due to concentration gradients. They considered a closed isothermal electrochemical cell and non-linear reaction kinetics, both analytically and numerically for large Rayleigh and Schmidt numbers, and found that mass transport in the free liquid electrolyte exhibited significant stratification, which sets up thin diffusion dominated layers in the vicinity of the electrodes and walls, where most of the mass transfer of the ions takes place. This stratification was shown to directly control the convective transport in the cell and the local ion concentrations along the electrodes, and so had a significant impact on cell performance.

The purpose of this investigation was to examine the case when the electrolyte is confined to a porous separator between the electrodes, as shown in Fig. 1. The main advantage of such a separator is its ability to prevent short

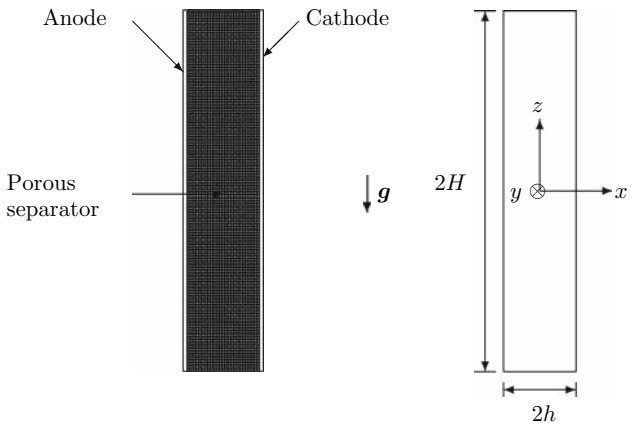

Fig. 1 Schematic illustration of an electrochemical cell with a porous separator, sandwiched between the two vertical electrodes. The cell geometry and the coordinate system are defined on the right

circuiting in the cell, arising from metallic bridges forming between the electrodes [10].

The objectives of this work were to: (i) derive the thickness of the boundary layers arising from the stratification at the electrodes a priori to computations; (ii) derive a reduced evolution equation, without sacrificing any of the salient physical features, which is several orders of magnitude faster to solve for than the full model; (iii) secure closed analytical solutions in the limit of small and large cell voltages. The benefits of these are the availability of closed-form analytical solutions for two important limits, a reduced evolution equation that is cheap to compute away from those limits, as well as an estimate of the boundary layer thicknesses that can aid in solving for the full model. The value of these is further enhanced by the fact that it becomes increasingly more difficult to solve a full mathematical model numerically as the potential difference across the cell is increased. The reason can be found in the non-linear reaction kinetics at the electrodes, which alter the local ion concentrations and thus the density of the liquid. These density variations give rise to the free convection, controlling most of the ion transfer to and from the electrodes, and in turn, the local ion concentrations at the electrodes.

2 Mathematical formulation of the basic problem

In the following, a two-dimensional electrochemical cell will be considered, comprising two electrodes of the same metal, denoted *Me*, separated by an inert porous medium, as depicted in Fig. 1. The porous separator is filled with a binary dilute liquid solution of the metal salt. For a closed-off cell, the reduction from three space dimensions to two is motivated by the porous nature of the separator, since changes in the dependent variables in the normal direction (y-direction) can be shown to be negligible. For electrochemical cells with flow of electrolyte through the cell (y-direction), the flow through the cell has to be sufficiently low, so that changes in the dependent variables in said direction are small enough for this approximation to hold. For example, this is the case in industrial electrorefining, where generally an open tank design with parallel-plate electrodes is employed. Here, a low flow rate through the cells allows the accumulated impurities in the electrolyte or cell slime to drop to the base, without coming into contact with the cathodes.

On applying a potential difference between the electrodes, with V_1 (anode) $> V_2$ (cathode), at $t > 0$, an electric current starts to flow in the cell. At the anode, the oxidation

$$Me \rightarrow Me^{z+} + ze^{-} \tag{1}$$

takes place, where z is the oxidation number of the metal *Me*. As the metal ions dissolve in the electrolyte, its density increases locally compared to the bulk electrolyte, whence the electrolyte adjacent to the anode starts to sink. On the cathode, on the other hand, dissolved metal ions are deposited through the reduction

$$Me^{z+} + ze^{-} \rightarrow Me \tag{2}$$

leading to a decrease of specific weight adjacent to the cathode and an upward movement of the electrolyte. Now, as the cell volume is constant and the electrolyte can be considered incompressible, a circular motion develops. The same scenario will occur if a current (galvanostatic electrolysis) is applied instead of a potential difference.

A proper description of the transport processes in the porous separator outlined above requires the introduction of volume averaged equations and associated superficial and intrinsic properties [11, 12]. For this purpose, let $\overline{\mathcal{P}}$ and $\overline{\mathcal{P}}^{(\mathrm{f})}$ denote the superficial and intrinsic averages of a property $\mathcal{P}$ (e.g., the concentration), defined as

$$\overline{\mathcal{P}} = \frac{1}{V}\int_{V^{(\mathrm{f})}} \mathcal{P}\mathrm{d}V, \tag{3}$$

$$\overline{\mathcal{P}}^{(\mathrm{f})} = \frac{1}{V^{(\mathrm{f})}}\int_{V^{(\mathrm{f})}} \mathcal{P}\mathrm{d}V. \tag{4}$$

Here, V is the total volume of the Representative Elementary Volume (REV), i.e., the volume over which the volume averaging is carried out, and $V^{(\mathrm{f})}$ is the volume of the fluid. Introducing the porosity as $\varphi = V^{(\mathrm{f})}/V$, the two averages are related through $\overline{\mathcal{P}} = \varphi\overline{\mathcal{P}}^{(\mathrm{f})}$. For the sake of brevity, we shall in the forthcoming analysis omit the overlining of the averaged properties, and note that all dependent variables are intrinsic, except for the velocity field of the electrolyte, $\boldsymbol{v}$, the total molar flux of species i, $\boldsymbol{N}^{(\mathrm{i})}$, and the current density $\boldsymbol{i}$. Further, the metal ion is labeled as species 1 and the corresponding anion as species 2.

In the porous separator, the equation describing conservation of momentum is assumed to be given by Darcy's law. If p denotes the pressure and $c^{(\mathrm{i})}$ the concentration of species i, Darcy's law together with the Boussinesq approximation takes the following form:

$$\boldsymbol{v} = -\frac{k}{\mu}\left(\nabla p + \left\{1 + \sum_{\mathrm{i}=1}^{2}\alpha^{(\mathrm{i})}\left[c^{(\mathrm{i})} - c_0^{(\mathrm{i})}\right]\right\}\rho_0 g\boldsymbol{e}_z\right), \tag{5}$$

where k is the permeability of the separator, μ is the viscosity of the electrolyte, $\alpha^{(\mathrm{i})}$ is the densification coefficient of species i, $c_0^{(\mathrm{i})}$ is the initial concentration of species i, chosen here as the reference concentration. The density ρ_0 is the initial density of the electrolyte, i.e.,

with $c^{(i)} = c_0^{(i)}$, and g denotes the acceleration due to gravity.

Liquid electrolytes are usually considered as incompressible; mathematically this implies that the velocity field must satisfy

$$\nabla \cdot \boldsymbol{v} = 0. \tag{6}$$

For binary or dilute electrolytes, the migration, diffusion and advection transport mechanisms are described by the Nernst–Planck law [13]. Denoting the scalar potential of the electrical field as ϕ, the Nernst–Planck law for the mass flux of species i, $\boldsymbol{N}^{(i)}$, can be written as

$$\boldsymbol{N}^{(i)} = -\frac{z^{(i)}F\varphi^{3/2}D^{(i)}}{RT}c^{(i)}\nabla\phi - \varphi^{3/2}D^{(i)}\nabla c^{(i)} + c^{(i)}\boldsymbol{v}, \quad i = 1, 2, \tag{7}$$

where $z^{(i)}$ is the oxidation number of species i, F is Faraday's constant, R is the gas constant, and $D^{(i)}$ is the diffusion constant of species i, which has been modified according to the Bruggeman formula, $\varphi^{3/2}$, see [14], to account for the porous nature of the separator. The temperature, T, of the electrolyte was assumed to be constant. Applying conservation of mass of species i yields

$$\varphi\frac{\partial c^{(i)}}{\partial t} + \nabla \cdot \boldsymbol{N}^{(i)} = 0. \tag{8}$$

Further, the transport of ionic species results in an electric current density, which can be expressed in terms of the total superficial mass fluxes of the ionic species, given by (7), as

$$\boldsymbol{i} = \sum_{i=1}^{2} Fz^{(i)}\boldsymbol{N}^{(i)}. \tag{9}$$

As the electrolyte is electrically neutral in every point, neglecting the electrode double layers, the total electric current is non-divergent, i.e., the local electric charge of the system should be equal to zero at all times; this condition can be stated as

$$\nabla \cdot \boldsymbol{i} = 0. \tag{10}$$

For a binary electrolyte the concentration fields are proportional to each other, since $z^{(1)}c^{(1)} + z^{(2)}c^{(2)} = 0$ at all times due to electroneutrality. It is thus sufficient to solve for one species only, so it is practical to introduce an artificial concentration c, given by

$$c = z^{(1)}c^{(1)} = -z^{(2)}c^{(2)}. \tag{11}$$

The re-scaled concentration field c has the advantage of automatically satisfying the local electroneutrality, (10), when reformulating the Eqs. 7–9 in terms of c. A reference concentration corresponding to c, c_0, is defined in the same way. Equation 8 can then, after eliminating ϕ, be recast as

$$\varphi\frac{\partial c}{\partial t} + \boldsymbol{v} \cdot \nabla c = D\nabla^2 c, \tag{12}$$

where the diffusivity, D, is defined by

$$D = \varphi^{3/2}\frac{\left[z^{(1)} - z^{(2)}\right]D^{(1)}D^{(2)}}{z^{(1)}D^{(1)} - z^{(2)}D^{(2)}}. \tag{13}$$

The proper boundary conditions for this system of coupled partial differential equations are, to start with,

$$\boldsymbol{v}(\pm h, z, t) \cdot \boldsymbol{e}_x = 0, \tag{14.1}$$

$$\boldsymbol{v}(x, \pm H, t) \cdot \boldsymbol{e}_z = 0, \tag{14.2}$$

which states that the normal component of the electrolyte velocity adjacent to a boundary vanishes. These conditions are a weaker form of the so-called no-slip conditions and are often used as boundary conditions in porous media.

As only species 1 takes part in the electrode reactions, the normal component of the mass flux vector of species 2 on the electrodes is equal to zero:

$$\boldsymbol{N}^{(2)} \cdot \boldsymbol{e}_x = 0, \quad x = \pm h. \tag{15}$$

For species 1, matters are more complicated: empirically, one finds that the concentration affects the local value of the electric current density at the electrodes. This coupling mechanism is responsible for the so-called limiting current phenomenon [13]. It is found that the relation between the electric current density and the concentrations at the electrodes is described quite well by the semi-empirical Butler–Volmer conditions [13], which for the present case take the following form:

$$\boldsymbol{i} \cdot \boldsymbol{e}_x|_{x=-h} = i_0\left\{\exp\left[\frac{z^{(1)}\gamma F}{RT}(V_1 - \phi)\right] - \frac{c^{(1)}}{c_0^{(1)}}\exp\left[-\frac{z^{(1)}(1-\gamma)F}{RT}(V_1 - \phi)\right]\right\}, \tag{16.1}$$

$$\boldsymbol{i} \cdot \boldsymbol{e}_x|_{x=h} = i_0\left\{\frac{c^{(1)}}{c_0^{(1)}}\exp\left[-\frac{z^{(1)}(1-\gamma)F}{RT}(V_2 - \phi)\right] - \exp\left[\frac{z^{(1)}\gamma F}{RT}(V_2 - \phi)\right]\right\}, \tag{16.2}$$

where i_0 is the exchange current density and γ is the transfer coefficient, which will be chosen as $\gamma = 1/2$ for simplicity. Returning to the definition of the current density, Eq. (9), and invoking the zero flux of species 2,

given by Eq. (15) on the electrodes, one finds the flux of species 1 at the electrodes:

$$\boldsymbol{N}^{(1)} \cdot \boldsymbol{e}_x = \frac{1}{Fz^{(1)}} \boldsymbol{i} \cdot \boldsymbol{e}_x, \quad x = \pm h.$$

Through the top and bottom of the cell, there is no net transfer of species 1 and 2; this condition can be stated as

$$\boldsymbol{N}^{(1)} \cdot \boldsymbol{e}_z = \boldsymbol{N}^{(2)} \cdot \boldsymbol{e}_z = 0, \quad z = \pm H. \tag{17}$$

Finally, the initial condition is taken to be

$$c^{(\mathrm{i})}(\boldsymbol{x}, 0) = c_0^{(\mathrm{i})}, \quad \mathrm{i} = 1, 2. \tag{18}$$

From this choice, it follows from (5) that $\boldsymbol{v}(\boldsymbol{x}, 0) = \boldsymbol{0}$.

3 Dimensionless variables

In this investigation, the initial value of the concentration, c_0 will be used as the scale of the concentration. This is not an obvious choice, but is an appropriate one, as can be verified a posteriori, if the concentration is not too small [3]. For algebraic simplicity, the case where $z^{(1)} = -z^{(2)} = 2$ will be considered; a corresponding analysis, for a different choice of $z^{(1)}$ and $z^{(2)}$, can be carried out with only minor modifications. Now, the following set of dimensionless variables is introduced:

$$\boldsymbol{x} = h\boldsymbol{x}^*, \quad t = \frac{h^2}{D} t^*, \quad \boldsymbol{i} = i_0 \boldsymbol{i}^* \tag{19.1}$$

$$\left[\phi - \frac{1}{2}(V_1 + V_2), \frac{1}{2}(V_1 - V_2)\right] = \frac{RT}{F}(\phi^*, \mathcal{V}^*), \tag{19.2}$$

$$c = c_0(1 + c^*), \quad \boldsymbol{N}^{(\mathrm{i})} = \frac{Dc_0}{h} \boldsymbol{N}^{(\mathrm{i})^*}, \tag{19.3}$$

$$\boldsymbol{v} = \frac{\rho_0 c_0 g k \left[\alpha^{(1)} + \alpha^{(2)}\right]}{2\mu} \boldsymbol{v}^*, \tag{19.4}$$

$$p + \rho_0 g z = \frac{\rho_0 c_0 g h \left[\alpha^{(1)} + \alpha^{(2)}\right]}{2} p^*. \tag{19.5}$$

Whilst scaling, four dimensionless parameters appear:

$$\mathrm{Ra} = \frac{\rho_0 c_0 g h k \left[\alpha^{(1)} + \alpha^{(2)}\right]}{2\mu D \varphi^{3/2}}, \quad \mathcal{H} = \frac{H}{h}, \tag{20.1}$$

$$\Gamma = \frac{2\left[D^{(1)} + D^{(2)}\right]}{D^{(1)} - D^{(2)}}, \quad \kappa = \frac{h i_0}{2D^{(1)} F c_0}. \tag{20.2}$$

The definition of dimensionless potentials in (19.2) is chosen in order to obtain a symmetric form of the dimensionless Butler–Volmer equation, see (28.1) and (28.2) below. Dropping *, the Eqs. 5, 6, and 12 formulated in terms of these dimensionless variables, become

$$\varphi \frac{\partial c}{\partial t} + \mathrm{Ra} \boldsymbol{v} \cdot \nabla c = \nabla^2 c, \tag{21}$$

$$\boldsymbol{v} = -\nabla p - c\boldsymbol{e}_z, \tag{22}$$

$$\nabla \cdot \boldsymbol{v} = 0. \tag{23}$$

The expression for the electric current density takes the form

$$\boldsymbol{i} = -\frac{2}{\kappa(\Gamma + 2)} [\Gamma(1 + c)\nabla\phi + \nabla c], \tag{24}$$

and the conservation of charge is rewritten as

$$\Gamma \nabla \cdot (1 + c)\nabla\phi + \nabla^2 c = 0. \tag{25}$$

This equation should be compared with Laplace's equation $\nabla^2\phi = 0$ for the electric potential in a homogeneous conductor. The more complicated appearance of (25) is due to two effects. Firstly, the inhomogeneous concentration field sets up a variable conductivity, which is quantified by the first term in the left-hand side of (25). Secondly, in an inhomogeneous electrolyte, transport of charge takes place also by means of diffusion, which is expressed by the second term.

The dimensionless counterparts of the boundary conditions for the fluid velocity at the walls (14) become

$$\begin{aligned} \boldsymbol{v}(\pm 1, z, t) \cdot \boldsymbol{e}_x &= 0, \\ \boldsymbol{v}(x, \pm\mathcal{H}, t) \cdot \boldsymbol{e}_z &= 0, \end{aligned} \tag{26.1}$$

and from (15), (16.1) and (16.2), with the scaling above, one arrives at

$$(1 + c)\frac{\partial\phi}{\partial x} = \frac{1}{2}\frac{\partial c}{\partial x}, \quad |x| = 1, \tag{27}$$

$$\left.\frac{\partial c}{\partial x}\right|_{x=-1} = -\kappa[\exp(\mathcal{V} - \phi) - (1 + c)\exp(-\mathcal{V} + \phi)], \tag{28.1}$$

$$\left.\frac{\partial c}{\partial x}\right|_{x=1} = -\kappa[(1 + c)\exp(\mathcal{V} + \phi) - \exp(-\mathcal{V} - \phi)]. \tag{28.2}$$

For notational brevity, the right-hand sides of the Butler–Volmer conditions above will sometimes be referred to as $-\lambda_-(c, \phi)$ (anode) and $\lambda_+(c, \phi)$ (cathode), respectively. The requirement of insulated horizontal walls (17) is given by

$$\frac{\partial c}{\partial x} = \frac{\partial \phi}{\partial x} = 0, \ |z| = \mathcal{H}, \tag{29}$$

and the dimensionless initial condition (18) is

$$c(\boldsymbol{x}, 0) = 0. \tag{30}$$

4 Parameters and dimensionless numbers

The physical and operational parameters are summarized in Table 1, and are chosen so as to keep consistency with [3], who studied the same system, but for a free electrolyte comprising a copper sulfate solution. These parameter values suggest that

$$\mathrm{Ra} = 1.74 \times 10^3, \Gamma = -10.3, \kappa = 7.20 \times 10^{-2},$$
$$\mathcal{H} = 5, \mathcal{V} \sim 1 - 10.$$

The large Rayleigh number, $\mathrm{Ra} \gg 1$, mirrors the stratification in the cell that arises due to the concentration variations, and will provide the basis for the model reductions in the following sections.

5 Numerical methods

To complement the upcoming reductions of the full mathematical model and provide verification of these, the full model was solved numerically with the finite-element based solver, Comsol Multiphysics [15]. The full numerical problem consists of Eqs. 21–23 together with (25), subject to the conditions (26.1–30) for the five dimensionless unknown variables $\boldsymbol{v} = (u, v)$, p, c, and ϕ. The computational domain, see Fig. 1, was resolved with a coarser mesh in the bulk and denser mesh close to the walls and electrodes. The thickness of the boundary layers close to the electrodes could be predicted based on the findings of the Prandtl-type solution in the next section. As an indication of the speed of computations, a typical transient run would require on the order of 10 CPU minutes on a 2 GHz PC with 1 GB of RAM for around 7×10^4 degrees of freedom, ensuring mesh-independent solutions. In general, it became increasingly more difficult to obtain fully converged solutions as $\mathcal{V}$ was increased. The reduced parabolic evolution equation together with the transcendental function and steady-state counterpart, to be outlined in Sect. 7, were solved with Comsol Multiphysics and Matlab [16]. Compared to the full numerical solution, the reduced equations could be computed within 1 CPU second or less—a reduction of close to three orders of magnitude in computational cost.

Table 1 Physical and operational parameters

Parameter	Value
ν	1.1×10^{-6} m^2 s^{-1}, [3]
D_1	7.2×10^{-10} m^2 s^{-1}, [3]
D_2	1.065×10^{-9} m^2 s^{-1}, [3]
i_0	1 A m^{-2}, [3]
F	9.6487×10^4 A s mol^{-1}
R	8.314 J mol^{-1} K^{-1}
k	3.5×10^{-9} m^2 (assumed)
$z^{(1)}$, $z^{(2)}$	2, –2
g	9.81 m s^{-2}
$\alpha_1 + \alpha_2$	1.678×10^{-4} m^3 mol^{-1}, [3]
c_0	10^2 mol m^{-3} (0.1 M), [3]
h	1×10^{-3} m
H	5×10^{-3} m
T	293 K (20 °C)

6 A Prandtl-type solution

A simple ansatz is employed to find a solution to the governing equations, away from the horizontal boundaries. This results in an order-of-magnitude estimate of the boundary-layer thickness of the velocity and concentration fields at the vertical walls and also exposes a natural length scale in the vertical coordinate. The reasoning in this section is a modified version of that in the work by Bark et al. [17], in which a corresponding study is made for a free liquid, i.e., using the incompressible Navier–Stokes equations instead of Darcy's law.

Firstly, the assumption that $\lambda_\pm$ are slowly varying functions of c and ϕ is made, so that $\lambda_\pm$ may be taken as prescribed constants; this choice corresponds to the case of linear reaction kinetics. Conservation of mass then gives $\lambda_+ = -\lambda_-$. In an attempt to solve the Eqs. 21–23, the following ansatz is made, which is attributed to Prandtl's model of mountain winds in stratified air:

$$\boldsymbol{v} = w(x)\boldsymbol{e}_z, c = \beta t - \mathcal{S}' z + \vartheta(x), \ p = p(z, t), \tag{31}$$

where w, ϑ and p are functions of one spatial variable to be determined from Darcy's law (22) and the equation describing the transport of mass (21). The numbers β and $\mathcal{S}'$ will be obtained from imposing a few natural requirements on the solution. It is important to note that the ansatz (31) is unreasonable near the top and bottom of the cell, i.e., for $z \approx \pm\mathcal{H}$. Fortunately, it turns out that using (31) in the whole cell introduces only minor errors as can be verified a posteriori. A more detailed discussion of this type of ansatz is given in [17].

The boundary conditions (28.1–28.2) are then transformed into

$$\vartheta'(-1) = -\lambda_-,\ \vartheta'(1) = \lambda_+. \tag{32}$$

The incompressibility condition is automatically satisfied by this ansatz, as is the condition of vanishing horizontal electrolyte velocity at the vertical cell boundaries. The corresponding condition at the horizontal cell boundaries can, however, not be applied to a solution of the kind suggested by this ansatz. The present solution is thus valid only away from the horizontal walls.

When the ansatz (31) is inserted into (21) and (22) one arrives at a system of coupled ordinary differential equations for $\vartheta(x)$ and $w(x)$:

$$\varphi\beta - \mathcal{S}'\mathrm{Ra}\, w = \vartheta'',\ w + \vartheta = -\Pi'_z, \tag{33}$$

where $\Pi = p + \beta z t - \frac{1}{2}\mathcal{S}'z^2$. This system has the solution

$$\vartheta(x) = Ae^{rx} + Be^{-rx} - \frac{\varphi\beta}{r^2} - \Pi'_z, \tag{34}$$

$$w(x) = -Ae^{rx} - Be^{-rx} + \frac{\varphi\beta}{r^2}, \tag{35}$$

$$\Pi'_z = \text{const.}, \tag{36}$$

where a new parameter, $r = (\mathcal{S}'\mathrm{Ra})^{1/2}$, and two constants of integration, A and B, have been introduced. The constants are determined from the boundary conditions (32) as

$$A = \frac{1}{r}\frac{\lambda_+ e^r + \lambda_- e^{-r}}{e^r - e^{-r}}e^{-r}, \tag{37.1}$$

$$B = \frac{1}{r}\frac{\lambda_+ e^{-r} + \lambda_- e^r}{e^r - e^{-r}}e^{-r}. \tag{37.2}$$

As the Rayleigh number Ra is much larger than unity, r is large accordingly. From computing approximate expressions for A and B in the limit where Ra is large, one obtains the following solutions for ϑ and w:

$$\vartheta(x) = \frac{1}{r}\left[\lambda_+ e^{-r(1-x)} + \lambda_- e^{-r(1+x)}\right] - \frac{\varphi\beta}{r^2} - \Pi'_z, \tag{38}$$

$$w(x) = -\frac{1}{r}\left[\lambda_+ e^{-r(1-x)} + \lambda_- e^{-r(1+x)}\right] + \frac{\varphi\beta}{r^2}. \tag{39}$$

These expressions fulfill the boundary conditions with an error of the order of e^{-2r}, and in what follows, all expressions will be truncated at the order of e^{-r}. Here, one important feature of this solution is revealed, namely the boundary-layer character exposed by the solution: the terms within the square brackets in $\vartheta(x)$ and $w(x)$ are dominant in vertical boundary-layers close to the electrodes with the thickness of r^{-1}. In the middle region of the cell, contributions of the order r^{-2} instead dominate.

To determine β, one may consider the net flux of the electrolyte through a horizontal plane in the cell, which has to be equal to zero due to incompressibility:

$$\int_{-1}^{1} w(x)\mathrm{d}x = 0, \tag{40}$$

Performing the integration using (39) yields

$$0 = 2\frac{\varphi\beta}{r^2} - \frac{\lambda_+ + \lambda_-}{r^2}, \tag{41}$$

with an error of $\mathcal{O}(e^{-r})$. Solving for β gives:

$$\beta = \frac{\lambda_+ + \lambda_-}{2\varphi}. \tag{42}$$

This result seems reasonable, since β should vanish if there is no net influx of mass; that is, if $\lambda_+ = -\lambda_-$, which is the case under consideration at present. However, if this is not the case, there exists a term in the solution for c that linearly increases or decreases the concentration with time.

The global change in the concentration originates from the balance between influx and outflux of ions at the electrodes. Thus, the solution must obey the following requirement of global conservation of mass:

$$\int_{-1}^{1}\int_{-\mathcal{H}}^{\mathcal{H}} \varphi c\mathrm{d}z\mathrm{d}x = t\int_{-\mathcal{H}}^{\mathcal{H}}[\vartheta'(1) - \vartheta'(-1)]\mathrm{d}z. \tag{43}$$

Substitution of the explicit expression for c as given by (39) into the equation above and performing the integral shows that (52) can be written as

$$4\varphi\beta t\mathcal{H} + \int_{-1}^{1}\int_{-\mathcal{H}}^{\mathcal{H}} \vartheta(x)\mathrm{d}z\mathrm{d}x = 4\varphi\beta t\mathcal{H}, \tag{44}$$

or

$$\int_{-1}^{1}\int_{-\mathcal{H}}^{\mathcal{H}} \vartheta(x)\mathrm{d}z\mathrm{d}x = 0. \tag{45}$$

When this is performed explicitly, one finds that $\Pi'_z = 0$, and thus, $\vartheta(x) = -w(x)$.

To determine $\mathcal{S}'$, one can formulate an argument due to a spatial mass balance: Eq. 21 can be written as

$$\varphi\frac{\partial c}{\partial t} + \nabla\cdot\boldsymbol{N} = 0, \tag{46}$$

where

$$\boldsymbol{N} = \mathrm{Ra}\boldsymbol{\nu}c - \nabla c \tag{47}$$

is the fictitious dimensionless mass flux vector governing the spatial distribution of c. Its interpretation in terms of the fluxes of species 1 and 2 together with the

expression for the dimensionless electric current density (24) is given by

$$\boldsymbol{N}^{(1)} = \frac{1}{2}\left[\boldsymbol{N} + \frac{\kappa(\Gamma+2)}{\Gamma-2}\boldsymbol{i}\right], \tag{48.1}$$

$$\boldsymbol{N}^{(2)} = \frac{1}{2}(\boldsymbol{N} - \kappa\boldsymbol{i}). \tag{48.2}$$

For a steady solution the total net mass flux through any horizontal layer in the cell should vanish, that is

$$\begin{aligned} 0 &= \int_{-1}^{1} \boldsymbol{e}_z \cdot \boldsymbol{N}\mathrm{d}x = \int_{-1}^{1} \boldsymbol{e}_z \cdot (\mathrm{Ra}\boldsymbol{v}c - \nabla c)\mathrm{d}x \\ &= \int_{-1}^{1} \left(-c_z' + \mathrm{Ra}wc\right)\mathrm{d}x. \end{aligned} \tag{49}$$

If the expressions (31) for c and w are substituted into (49), integration followed by some algebra yields

$$\mathcal{S}' = \left(\frac{\lambda_+^2 + \lambda_-^2}{4}\right)^{2/5} \mathrm{Ra}^{-1/5} + \mathcal{O}\left(\mathrm{Ra}^{-3/5}\right). \tag{50}$$

This result exposes an important feature of the solution, namely the existence of a natural length scale in the vertical coordinate, since $|c_z'| \sim \mathrm{Ra}^{-1/5}$. The result (50) also implies that

$$r = (\mathcal{S}'\mathrm{Ra})^{1/2} \sim \mathrm{Ra}^{2/5}, \tag{51}$$

whence the vertical boundary-layer thickness, r^{-1}, is of the order $\mathrm{Ra}^{-2/5}$. These results should be compared with the results obtained in [17] with the incompressible Navier–Stokes equations, where the vertical length scale was shown to be $\sim \mathrm{Ra}^{-1/9}$, and where the vertical boundary-layer thickness was determined as being of the order of $\sim \mathrm{Ra}^{-2/9}$.

The numerical solution of the steady version of the problem (21–23) together with (25), subject to the conditions (26.1–30) supports these results, see Fig. 2.The order-of-magnitude estimates of the vertical length scale (50) and the vertical boundary-layer thickness (51) will form the basis upon which the next section rests.

7 Extension to non-linear reaction kinetics

In the previous section it was found that for large values of the Rayleigh number, the concentration in the bulk of the cell varies vertically on a length scale of the order of $\mathrm{Ra}^{-1/5}$. It was also shown, that the concentration, as well as the velocity, exhibits a boundary-layer character close to the electrodes, with the corresponding boundary-layer thickness $\mathrm{Ra}^{-2/5}$. It is thus natural to introduce a small expansion parameter $\varepsilon = \mathrm{Ra}^{-1/5}$ and to use the following variables

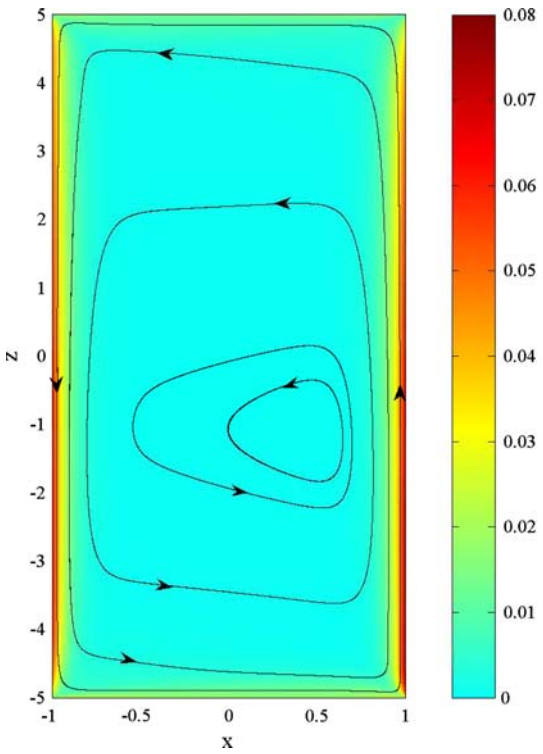

Fig. 2 Streamlines and velocities (v) of the electrolyte for Ra = 1.74 $\times 10^3$, $\Gamma = -10.3$, $\kappa = 7.20 \times 10^{-2}$, $\mathcal{H} = 5, \mathcal{V} = 3$. The boundary layers adjacent to the anode ($x = -1$) and cathode ($x = 1$) are clearly visible

$$\eta_\pm = \frac{1 \mp x}{\epsilon^2}, \quad \zeta = \epsilon z, \; \tau = \epsilon^2 t. \tag{52}$$

In the numerical results to be presented later, $\varepsilon = 0.225$, as follows from the value of Ra given in Sect. 4. Here the 'stretched' horizontal coordinates $\eta_\pm$ are of the order of unity in the vertical boundary layers at the cathode and anode, respectively. The 'slow' vertical coordinate ζ is chosen in such a way that the variation of the concentration with ζ is of the order of unity. The new time scale introduced in τ above is chosen in such a way that the local rate-of-change of the concentration will be of the same order of magnitude as the vertical diffusive transport of mass. With these variables, and based on the results obtained in the previous section, a new ansatz is formulated according to

$$c = -\mathcal{C}(\zeta,\tau) + \epsilon^2[\vartheta_+(\mathcal{C},\eta_+) + \vartheta_-(\mathcal{C},\eta_-)] + \ldots \tag{53}$$

$$\begin{aligned} \boldsymbol{v} = (&\epsilon^5[u_+(\mathcal{C},\eta_+) + u_-(\mathcal{C},\eta_-)], \epsilon^2[w_+(\mathcal{C},\eta_+) + w_-(\mathcal{C}.\eta_-)]) \\ &+ \ldots \end{aligned} \tag{54}$$

In these expressions, the functions ϑ and w are redefined as

$$\vartheta_{\pm} = -w_{\pm} = \left(\frac{\partial \mathcal{C}}{\partial \zeta}\right)^{-1/2} \lambda_{\pm}(c,\phi) \exp\left[-\left(\frac{\partial \mathcal{C}}{\partial \zeta}\right)^{1/2} \eta_{\pm}\right] + \mathcal{O}(\epsilon), \tag{55}$$

and as a consequence:

$$r = \epsilon^{-2} \left(\frac{\partial \mathcal{C}}{\partial \zeta}\right)^{1/2}. \tag{56}$$

For this new ansatz, $\mathcal{C} \sim 1$ for all ζ and τ, and $\vartheta_{\pm}$, $u_{\pm}$ and $w_{\pm} \sim 1$ when $\eta_{\pm} \sim 1$. It is clear that for the assumption of slow vertical variation to be fulfilled, and for the boundary-layer character of the solution to be well-defined:

$$\epsilon^4 \ll \frac{\partial \mathcal{C}}{\partial \zeta} \ll \epsilon^{-1}. \tag{57}$$

The functions $\lambda_{\pm}(c, \phi)$ are no longer regarded as constants, but instead dependent on the concentration and the electrical potential in the electrolyte at the electrodes, as quantified by the Butler–Volmer conditions (28.1) and (28.2). The order-of-magnitude of the horizontal velocity component, ε^5, is found from the incompressibility condition. The ansatz (53) and (54) is analogous to the one used in [3].

In order to derive an evolution equation for $\mathcal{C}$, one can consider the total net mass flux of species 1 into a specified control volume. The control volume that will be used here is the thin horizontal strip between the two horizontal planes $z = z'$ and $z = z' + \delta z$. If the horizontal average (or rather, twice the horizontal average) per unit length in the y-direction of an arbitrary quantity, say $\mathcal{Q}(x)$, denoted by $\langle \mathcal{Q} \rangle$ is defined according to

$$\langle \mathcal{Q} \rangle \equiv \int_{-1}^{1} \mathcal{Q}(x) \mathrm{d}x, \tag{58}$$

the total mass of species 1 in the thin horizontal strip can be approximated with $\varphi \langle c^{(1)} \rangle \delta z$. Further, conservation of species 1 requires, in the limit where δz tends to zero, that

$$\epsilon^2 \varphi \frac{\partial}{\partial \tau} \left\langle c^{(1)} \right\rangle = -\epsilon \frac{\partial}{\partial \zeta} \left\langle \boldsymbol{N}^{(1)} \cdot \boldsymbol{e}_z \right\rangle + \left(\boldsymbol{N}^{(1)}|_{x=-1} - \boldsymbol{N}^{(1)}|_{x=1} \right) \cdot \boldsymbol{e}_x. \tag{59}$$

The aim is now to formulate this partial differential equation into one containing $\mathcal{C}$, τ and ζ only: one obtains from relation (48.2)

$$\boldsymbol{N}^{(1)} \cdot \boldsymbol{e}_x \big|_{x=\pm 1} = \frac{1}{2} \left(\boldsymbol{N} \cdot \boldsymbol{e}_x + \frac{\kappa(\Gamma + 2)}{\Gamma - 2} \boldsymbol{i} \cdot \boldsymbol{e}_x \right) \Bigg|_{x=\pm 1}, \tag{60}$$

and, since there is no mass flux of species 2 through the electrodes (15), one obtains

$$\boldsymbol{N} \cdot \boldsymbol{e}_x|_{x=\pm 1} = \kappa \boldsymbol{i} \cdot \boldsymbol{e}_x|_{x=\pm 1}. \tag{61}$$

Thus, one can write

$$\boldsymbol{N}^{(1)} \cdot \boldsymbol{e}_x \big|_{x=\pm 1} = \frac{\kappa \Gamma}{\Gamma - 2} \boldsymbol{i} \cdot \boldsymbol{e}_x \Bigg|_{x=\pm 1}. \tag{62}$$

The right-most term in (59) can now be written as

$$\frac{\kappa \Gamma}{\Gamma - 2} \left(\boldsymbol{i} \cdot \boldsymbol{e}_x|_{x=-1} - \boldsymbol{i} \cdot \boldsymbol{e}_x|_{x=1} \right) = -\frac{\kappa \Gamma}{\Gamma - 2} \left\langle \frac{\partial \boldsymbol{i} \cdot \boldsymbol{e}_x}{\partial x} \right\rangle. \tag{63}$$

Moreover, as the electric current density is non-divergent, $\boldsymbol{i}$ has to obey the following relation:

$$\frac{\partial \boldsymbol{i} \cdot \boldsymbol{e}_x}{\partial x} = -\epsilon \frac{\partial \boldsymbol{i} \cdot \boldsymbol{e}_z}{\partial \zeta}, \tag{64}$$

which leads to

$$-\frac{\kappa \Gamma}{\Gamma - 2} \left\langle \frac{\partial \boldsymbol{i} \cdot \boldsymbol{e}_x}{\partial x} \right\rangle = \epsilon \frac{\kappa \Gamma}{\Gamma - 2} \left\langle \frac{\partial \boldsymbol{i} \cdot \boldsymbol{e}_z}{\partial \zeta} \right\rangle = \epsilon \frac{\kappa \Gamma}{\Gamma - 2} \frac{\partial \langle \boldsymbol{i} \cdot \boldsymbol{e}_z \rangle}{\partial \zeta}. \tag{65}$$

By observing that $z^{(1)} = 2$ and thus, according to (11), $c = 2c^{(1)}$, one obtains $\langle c^{(1)} \rangle = -\mathcal{C} + \mathcal{O}(\epsilon)$, so that (59) can be rewritten as

$$\epsilon \varphi \frac{\partial \mathcal{C}}{\partial \tau} = \frac{1}{2} \frac{\partial}{\partial \zeta} \left(\langle \boldsymbol{N} \cdot \boldsymbol{e}_z \rangle - \kappa \langle \boldsymbol{i} \cdot \boldsymbol{e}_z \rangle \right). \tag{66}$$

From the definition (47) of $\boldsymbol{N}$, and with the new ansatz for $(\vartheta_{\pm}, w_{\pm})$, one finds that

$$\langle \boldsymbol{N} \cdot \boldsymbol{e}_z \rangle = 2\epsilon \frac{\partial \mathcal{C}}{\partial \zeta} + \frac{1}{\epsilon} \langle (\vartheta_+ + \vartheta_-)(w_+ + w_-) \rangle. \tag{67}$$

The rightmost term in the above equation can be calculated from (55) to sufficient order, and the result is

$$\langle (\vartheta_+ + \vartheta_-)(w_+ + w_-) \rangle = -\epsilon^2 \frac{\lambda_+^2 + \lambda_-^2}{2} \left(\frac{\partial \mathcal{C}}{\partial \zeta} \right)^{-3/2} + \mathcal{O}(\epsilon^3). \tag{68}$$

The evolution equation for $\mathcal{C}$ then takes the form

$$\varphi \frac{\partial \mathcal{C}}{\partial \tau} = \frac{\partial}{\partial \zeta} \left[\frac{\partial \mathcal{C}}{\partial \zeta} - \frac{\lambda_+^2 + \lambda_-^2}{4} \left(\frac{\partial \mathcal{C}}{\partial \zeta} \right)^{-3/2} \right] - \frac{\kappa}{2\epsilon} \frac{\partial}{\partial \zeta} \langle \boldsymbol{i} \cdot \boldsymbol{e}_z \rangle. \tag{69}$$

In order to express this equation in terms of $\mathcal{C}$, τ and ζ only, expressions for $\langle \boldsymbol{i} \cdot \boldsymbol{e}_z \rangle$ and $\lambda_+^2 + \lambda_-^2$ in terms of $\mathcal{C}$ have to be secured. These expressions will turn out to depend on the explicit form of the electric potential ϕ.

In order to solve Eq. 25 for the electric potential ϕ, this variable is expanded into an outer and an inner expansion, respectively, according to

$$\phi = \phi_0(x,\zeta,\tau) + \epsilon^2\phi_1(x,\zeta,\tau) + .., \quad \begin{cases} |x| < 1 - \mathcal{O}(\epsilon^2) \\ |\zeta| < \mathcal{L} - \mathcal{O}(\epsilon) \end{cases} \tag{70.1}$$

$$\phi = \psi_{0\pm}(\eta_\pm,\zeta,\tau) + \epsilon^2\psi_{1\pm}(\eta_\pm,\zeta,\tau) + .., \quad \begin{cases} \eta_\pm \sim 1, \\ |\zeta| < \mathcal{L} - \mathcal{O}(\epsilon), \end{cases} \tag{70.2}$$

where expression (70.1) is valid outside the vertical boundary layers at the electrodes, whereas expression (70.2) holds within these boundary layers. The aim is now to find these expressions explicitly, and to tie them together within a uniformly valid expansion that will tend to (70.1) outside the boundary layers, and to (70.2) next to the electrodes; see e.g., [18] and [3] for details of the closely related problem with a free liquid electrolyte. In fact, for the electric potential, but not for the concentration, the analysis is identical to that in [3].

These expansions are substituted into Eq. 25, resulting in differential equations for ϕ and $\psi_\pm$, respectively:

$$\frac{\partial^2\phi_0}{\partial x^2} = 0, \tag{71.1}$$

$$\Gamma(1-\mathcal{C})\frac{\partial^2\phi_1}{\partial x^2} + \Gamma\frac{\partial}{\partial\zeta}\left[(1-\mathcal{C})\frac{\partial\phi_0}{\partial x}\right] - \frac{\partial^2\mathcal{C}}{\partial\zeta^2} = 0, \tag{71.2}$$

$$\Gamma(1-\mathcal{C})\frac{\partial^2\psi_{0\pm}}{\partial\eta_\pm^2} = 0, \tag{71.3}$$

$$\frac{\partial^2\psi_{1\pm}}{\partial\eta_\pm^2} + \frac{\partial^2\vartheta_\pm}{\partial\eta_\pm^2} = 0. \tag{71.4}$$

These equations are readily solved, and after matching the inner and outer expansions, one arrives at the following uniformly valid expansion:

$$\begin{aligned}\phi \;=\; & \Phi_0(\zeta,\tau) + \Phi_1(\zeta,\tau)x + \epsilon^2[\Phi_2(\zeta,\tau) + \Phi_3(\zeta,\tau)x] \\ & - \epsilon^2\frac{1}{\Gamma(1-\mathcal{C})}\left\{\frac{\partial}{\partial\zeta}\left[\Gamma(1-\mathcal{C})\left(\frac{x^2}{2}\frac{\partial\Phi_0}{\partial\zeta} + \frac{x^3}{6}\frac{\partial\Phi_1}{\partial\zeta}\right)\right.\right. \\ & \left.\left. - \frac{x^2}{2}\frac{\partial\mathcal{C}}{\partial\zeta}\right] - (\vartheta_+ + \vartheta_-)\right\},\end{aligned} \tag{72}$$

where the unknown functions $\Phi_k, k = 0,\ldots,3$, can be determined in terms of $\mathcal{C}$ from the boundary conditions at the electrodes. In the present work, the analysis is terminated at $\mathcal{O}(\epsilon^2)$, i.e., only Φ_0 and Φ_1 will be determined. The expression (72) is then inserted into the boundary condition (27), whence

$$\frac{\partial\vartheta_\pm}{\partial\eta_\pm} = \mp\frac{2\Gamma(1-\mathcal{C})}{\Gamma+2}\Phi_1,\; x = \pm 1, \tag{73}$$

which, when substituted into the Butler-Volmer conditions (28.1) and (28.2) yields

$$\begin{aligned}\frac{2\Gamma(1-\mathcal{C})}{\Gamma+2}\Phi_1 \;=\; & -\kappa[\exp(\mathcal{V} - \Phi_0 + \Phi_1) \\ & -(1-\mathcal{C})\exp(\Phi_0 - \Phi_1 - \mathcal{V})],\end{aligned} \tag{74.1}$$

$$\begin{aligned}\frac{2\Gamma(1-\mathcal{C})}{\Gamma+2}\Phi_1 \;=\; & -\kappa[(1-\mathcal{C})\exp(\Phi_0 + \Phi_1 + \mathcal{V}) \\ & -\exp(-\mathcal{V} - \Phi_0 - \Phi_1)].\end{aligned} \tag{74.2}$$

The solution for Φ_0 is

$$\Phi_0 = -\frac{1}{2}\ln(1-\mathcal{C}), \tag{75}$$

and Φ_1 can be determined from the following transcendental equation:

$$\Phi_1 = -\frac{\kappa(\Gamma+2)}{\Gamma(1-\mathcal{C})^{1/2}}\sinh(\Phi_1 + \mathcal{V}). \tag{76}$$

Furthermore, the term $\langle \boldsymbol{i}\cdot\boldsymbol{e}_z\rangle$ can be calculated from (24):

$$\langle \boldsymbol{i}\cdot\boldsymbol{e}_z\rangle = -\frac{2\epsilon(\Gamma-2)}{\kappa(\Gamma+2)}\frac{\partial\mathcal{C}}{\partial\zeta}; \tag{77}$$

for $\lambda_\pm$ one gets

$$\lambda_+ = -\lambda_- + \mathcal{O}(\epsilon) = \frac{2\Gamma(1-\mathcal{C})}{(\Gamma+2)}\Phi_1 + \mathcal{O}(\epsilon), \tag{78}$$

and thus the evolution equation for $\mathcal{C}(\zeta,\tau)$ becomes

$$\varphi\frac{\partial\mathcal{C}}{\partial\tau} = \frac{\partial}{\partial\zeta}\left[\frac{2\Gamma}{\Gamma+2}\frac{\partial\mathcal{C}}{\partial\zeta} - \frac{2\Gamma^2(1-\mathcal{C})^2}{(\Gamma+2)^2}\Phi_1^2(\mathcal{C})\left(\frac{\partial\mathcal{C}}{\partial\zeta}\right)^{-3/2}\right]. \tag{79}$$

It is instructive to compare this non-linear parabolic equation with the corresponding equation found in [3] for a free liquid electrolyte: firstly, the evolution equation for the concentration obtained in that work differs from (79) in terms of the numerical coefficients; secondly, and most importantly, the exponent of the derivative $\partial\mathcal{C}/\partial\zeta$ was found to be –5/4 for a free liquid electrolyte, as compared to –3/2 for the porous separator. The latter difference will give rise to a qualitative difference in the asymptotic stratification, which will be discussed in the next section. Furthermore, for the case of a free electrolyte, the 'diffusivity', is for small values of $\partial\mathcal{C}/\partial\zeta$ of the order of

$(\partial\mathcal{C}/\partial\zeta)^{-9/4}$.In contrast, the corresponding diffusivity for the porous separator is instead $(\partial\mathcal{C}/\partial\zeta)^{-5/2}$, which is thus larger for small values of $\partial\mathcal{C}/\partial\zeta$. This means that for a weak stratification, the 'memory' of the solution is very short. This observation, which will prove useful for determining the initial conditions later, is discussed further in [17].

The boundary conditions that are required for (79) should prescribe the values of $\mathcal{C}(\zeta)$ when $\zeta = \pm\epsilon\mathcal{H} \equiv \pm\mathcal{L}$. In addition, the aspect ratio, $\mathcal{H}$, is here considered to be $\sim\varepsilon^{-1}$, whence $\mathcal{L}$ must be ~ 1. As the assumption of a slow vertical variation of $\mathcal{C}$ breaks down at the top and bottom regions of the cell, where horizontal boundary layers appear, there is a priori no accessible boundary conditions for $\mathcal{C}(\zeta)$ in these regions. However, it is reasonable to require, since species 2 is not produced or consumed at the electrodes, that for all values of τ, $\langle \boldsymbol{N}^{(2)} \cdot \boldsymbol{e}_z \rangle = 0$ at the top or bottom regions of the cell. As pointed out by Bark and Alavyoon in [3], the terms within the square brackets on the right-hand side of (79) corresponds to $\langle \boldsymbol{N}^{(2)} \cdot \boldsymbol{e}_z \rangle$, which is thus equal to zero at the horizontal boundaries at the top- and bottom of the cell. Following [3], we require that this also holds for $\mathcal{C}(\zeta)$ at $\zeta = \pm\mathcal{L}$. Equating the terms within the square brackets to zero, one obtains the boundary condition

$$\frac{\partial\mathcal{C}}{\partial\zeta} = \left(\frac{\Gamma}{\Gamma+2}\right)^{2/5} [(1-\mathcal{C})|\Phi_1(\mathcal{C})|]^{4/5}, \ \zeta = \pm\mathcal{L} \tag{80}$$

The initial condition should be obtained by matching the solution to (79) and (76) to an inner solution in time, i.e., a solution on the timescale $t = h^2 t^*/D \sim 1$, see definition (19.1). Such a solution is not accessible in the present work. However, in [17], where a similar difficulty is encountered, it was shown that an equation of the type of (79) soon looses its memory of an initial condition with not too steep concentration gradients, due to the large diffusivity discussed above. This suggests that as long as the initial condition does not introduce a strong stratification, it can be chosen quite freely. Further, the initial condition should satisfy the global conservation of mass and provide, for numerical reasons, at least a continuous first order derivative of $\mathcal{C}$. For this purpose, an initial condition of the form

$$\mathcal{C}(\zeta,0) = \mathfrak{k}_1\zeta, \quad |\zeta| < \mathcal{L}-\delta, \tag{81.1}$$

$$\mathcal{C}(\zeta,0) = \mathrm{sign}(\zeta)\left[\mathfrak{k}_2 + \mathfrak{k}_3 \exp\left(-\frac{\mathcal{L}-|\zeta|}{\delta}\right)\right], \quad |\zeta| \geq \mathcal{L}-\delta, \tag{81.2}$$

can be employed. Here, δ is an assumed thickness of the initial horizontal boundary layers at the top and bottom of the cell, and the constants $\mathfrak{k}_2$ and $\mathfrak{k}_3$ are determined from matching (81.1) and (81.2) and their first derivatives with respect to ζ at $\zeta = \mathcal{L}-\delta$. One then obtains

$$\mathfrak{k}_2 = \mathfrak{k}_1(\mathcal{L}-2\delta), \tag{82.1}$$

$$\mathfrak{k}_3 = \mathfrak{k}_1\delta\exp(1), \tag{82.2}$$

and $\mathfrak{k}_1$ is determined from boundary condition (80) for the chosen value of δ.

The solution to the one-dimensional parabolic PDE (79) and transcendental function (76), subject to the initial and boundary conditions (81.1), (81.2) and (80), together with the full numerical solution are depicted in Figs. 3–5.

Here, several features are apparent: foremost is the good agreement between the reduced model and the full numerical counterpart. In Fig. 3, where the vertical concentration in the center of the cell ($x = 0$) is depicted, quite moderate deviations between the reduced model and full numerical model predictions can be seen close to the lower wall of the cell, as the approximate approach looses its validity there. Somewhat surprising, however, is the good agreement close to the upper wall where the reduced model is also invalid. Further, as expected, the concentration profile is more uniform at low voltages and becomes increasingly less so at higher voltages, as more and more cations are dissolved at the anode for higher currents, increasing the liquid density locally, causing it to move to the bottom of the cell. In the horizontal direction of the cell ($z = 0$), the concentration is constant in the bulk, as can be inferred from Fig. 4. In the vicinity of the anode, however, the concentration increases due to the dissolution from the metal, and conversely, on the cathode, it decreases due to the metal consumption. The thickness of the dimensionless

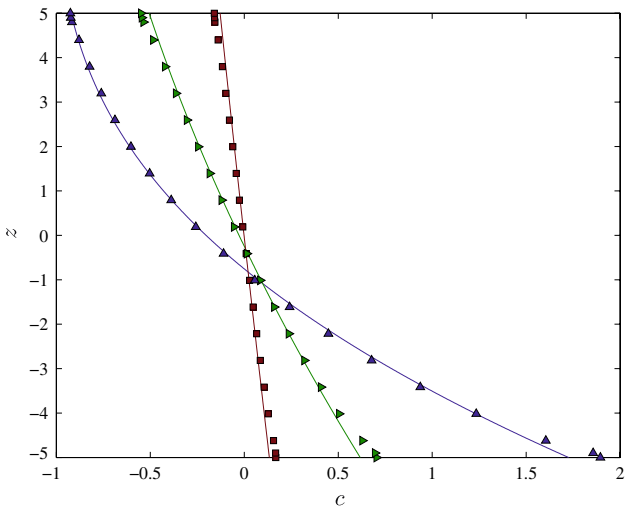

Fig. 3 The vertical concentration profile: c as a function of z. Comparisons between the steady-state solutions to the simplified evolution Eq. 79 (solid curves) and the corresponding solutions of the full problem, for $\mathcal{V} = 1$ (□), $\mathcal{V} = 3$ (▷), and $\mathcal{V} = 5$ (△), for $x = 0$

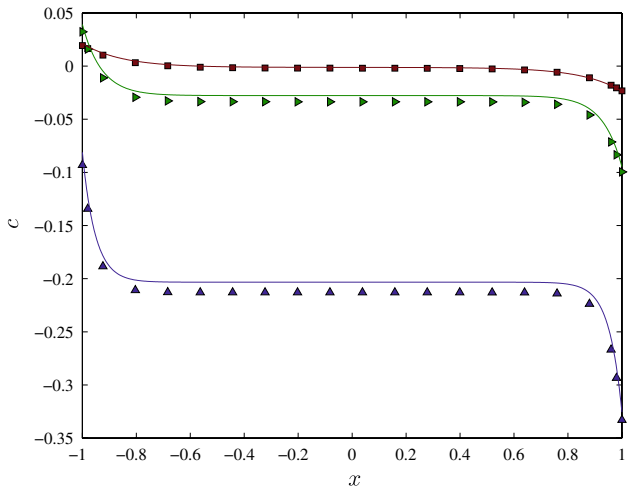

Fig. 4 The horizontal variation of the concentration: c as a function of x for $z = 0$. Comparisons between the steady-state solutions to the simplified evolution Eq. 79 (solid curves) and the corresponding solutions of the full problem, for $\mathcal{V} = 1$ (□), $\mathcal{V} = 3$ (▷), and $\mathcal{V} = 5$ (△)

boundary layers at the electrodes is around 0.1, which is of the same order of magnitude as the earlier predicted thickness of $\mathrm{Ra}^{-2/5}$. Increasing cell voltage sees steeper concentration gradients close to the electrodes and a decreasing overall steady-state concentration in the middle of the cell. The steep concentration variations in the stratification layers give rise to the free convection as the denser fluid at the anode flows downwards, and the less dense fluid at the cathode flows upwards. This behavior is illustrated in Fig. 5 for the vertical velocity. The magnitude of the vertical velocity is the highest at the electrodes due to the slip conditions and decreases towards the bulk, where there are no horizontal concentration variations, and hence no driving force for a convective motion. Further, the velocity increases with increased cell voltages as the concentration gradients then become more pronounced at the electrodes.

From the definition of the electric current density (24), the concentration (53), the boundary conditions (28.1), (28.2) and (27) and formula (78), the current density in the normal direction at the anode can be determined as

$$\boldsymbol{i} \cdot \boldsymbol{e}_x|_{x=-1} = -\frac{2\Gamma(1-\mathcal{C})}{\kappa(\Gamma+2)}\Phi_1. \tag{83}$$

The local current density along the anode mirrors the concentration profile, as can be inferred from Fig. 6, where the current density is almost constant for the low cell voltage $\mathcal{V} = 1$. Increasing cell voltages lead to a more non-uniform distribution, for which the local current density is higher near the bottom of the cell and decreases upwards along the anode. While it is desirable to run electrochemical applications, such as electrorefining or electroplating, at high cell voltages for increased rates of production, the resulting non-uniform current density distribution limits the operating voltage as an even current density distribution is of importance for the final product.

Thus far, the reduced model has been found to agree well with the full numerical counterpart and at a computational cost that is significantly lower, as discussed in Sect. 5. This can be attributed to the reduction in spatial dimensionality of the simplified model. Once $\mathcal{C}(\zeta, \tau)$ is known, an approximate two-dimensional solution, valid

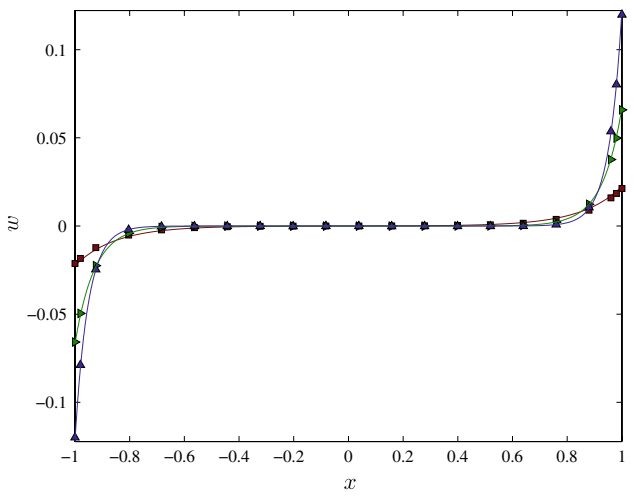

Fig. 5 The horizontal variation of the vertical velocity: w as a function of x at $z = 0$. Comparisons between the steady-state solutions to the simplified evolution Eq. 79 (solid curves) and the corresponding solutions of the full problem, for $\mathcal{V} = 1$ (□), $\mathcal{V} = 3$ (▷), and $\mathcal{V} = 5$ (△)

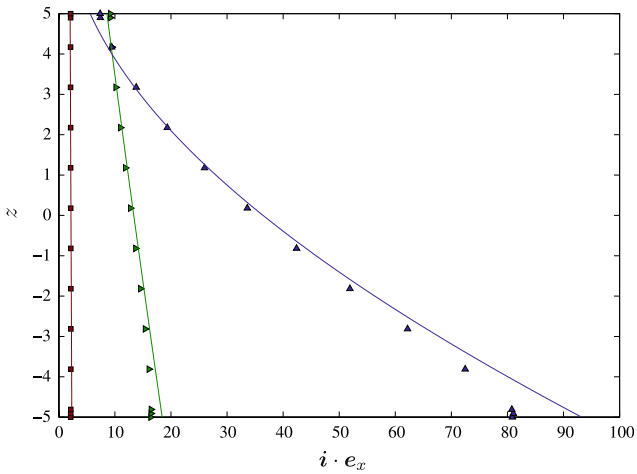

Fig. 6 The normal component of the electric current density: $\boldsymbol{i} \cdot \boldsymbol{e}_x$ at the anode ($x = -1$) as a function of the vertical coordinate z. Comparisons between the steady-state solutions, in terms of (83), of the simplified evolution equation (79) (solid curves) and the corresponding electric current density that stems from the solution to the full problem, for $\mathcal{V} = 1$ (□), $\mathcal{V} = 3$ (▷), and $\mathcal{V} = 5$ (△)

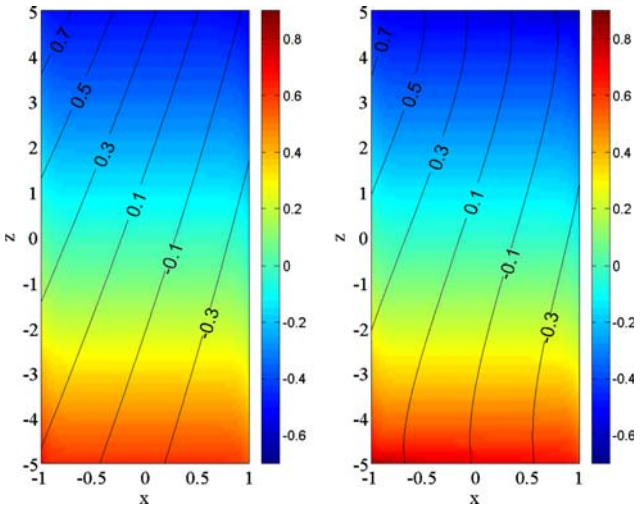

Fig. 7 Contours of constant potential in the separator, together with a field plot of the concentration, for the case $\mathcal{V} = 3$. The left figure illustrates the solution of the simplified theory according to (79), whereas the corresponding solution of the full numerical problem is shown in the right figure

outside the horizontal boundary layers on the top and bottom walls, can easily be computed from Eqs. 53–55, 72 and 76 together with (80). Such a solution, extended to the top and bottom walls, is shown in Fig. 7 for the cell potential and concentration. Clearly, the reduced model predictions follow the full numerical solution closely, except, as expected, at the lower and upper walls; however, this error is modest.

Finally, the transient behavior of the electrolysis is demonstrated in Fig. 8 for the reduced model in the middle of the cell. As outlined above, it is possible to construct an approximate two-dimensional solution at every time step. It

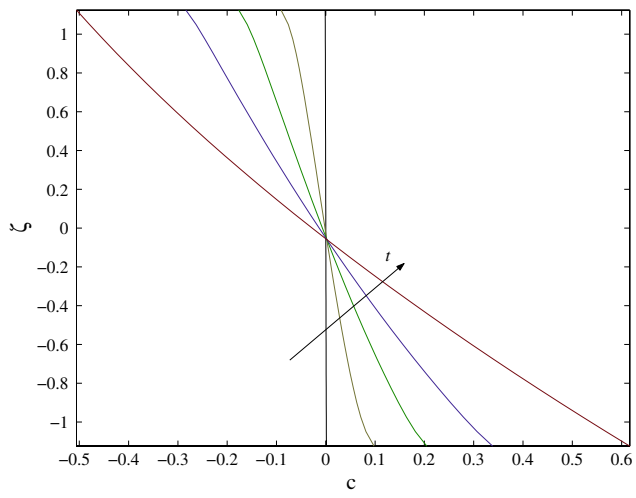

Fig. 8 Unsteady electrolysis. The evolution toward steady state described by the evolution Eq. 79 at $x = 0$ for $\mathcal{V} = 3$, at $t = 0$, 0.1, 0.5, 1, and 5

is apparent from this picture that the error introduced by the *ad hoc* initial condition comprised by (81.1) and (81.2) decays rather rapidly. As pointed out in [17], this is due to stratification increasing with time.

8 Approximate steady solutions

The steady solution is obtained by integrating the right-hand side of (79) twice with respect to ζ. The first integration is trivial. Taking into account that the net mass flux density of species 2 at any horizontal cross-section of the cell is zero determines the constant of integration. One finds that

$$\frac{d\mathcal{C}}{d\zeta} = \left(\frac{\Gamma}{\Gamma+2}\right)^{2/5} [(1-\mathcal{C})|\Phi_1(\mathcal{C})|]^{4/5}. \tag{84}$$

An exact solution to this differential equation coupled with the transcendental equation for Φ_1 is most likely out of reach; we can, however, secure approximate solutions via perturbation methods. As the non-linearity of the solution, introduced by the non-linear reaction kinetics, increases with higher applied voltages, a steady solution in the limit where $\mathcal{V}$ is large is of interest. For such a solution, an approximate expression for Φ_1 in the present limit is required. From iteration, one finds from (76) the following expression in this limit:

$$\Phi_1(\mathcal{C}) = -\mathcal{V} + \operatorname{arcsinh}\left[\sigma(1-\mathcal{C})^{1/2}\mathcal{V}\right] + \ldots \tag{85}$$

where

$$\sigma \equiv \frac{\Gamma}{\kappa(\Gamma+2)} \tag{86}$$

has been introduced. Defining a new vertical coordinate according to $\tilde{\zeta} \equiv (\kappa\sigma)^{2/5}\zeta, |\tilde{\zeta}| \le (\kappa\sigma)^{2/5}\mathcal{L} \equiv \tilde{\mathcal{L}}$, the Eq. 84 can be written as

$$\frac{d\mathcal{C}}{d\tilde{\zeta}} = \mathcal{V}^{4/5}(1-\mathcal{C})^{4/5}\left\{1 - \frac{4}{5\mathcal{V}}\operatorname{arcsinh}\left[\sigma(1-\mathcal{C})^{1/2}\mathcal{V}\right]\right\} + \ldots \tag{87}$$

Assuming an asymptotic form according to $1-\mathcal{C} = C_0 + C_1 + \ldots$, with $C_1 \ll C_0$ for large $\mathcal{V}$, one arrives at the following expression for C_0:

$$C_0(\tilde{\zeta}) = \mathcal{V}^4 \frac{(\tilde{\zeta}_0 - \tilde{\zeta})^5}{5^5}, \tag{88}$$

where $\tilde{\zeta}_0$ is a constant of integration. Thus, to lowest order, the concentration is given by a fifth-order polynomial in the vertical coordinate; the correction term C_1 is calculated in the appendix. Expression (88) should be compared to the

corresponding ninth-order polynomial found by Bark and Alavyoon in [3]. The constant $\tilde{\zeta}_0$ is determined from the constraint that C_0 has to fulfill the requirement of global conservation of mass

$$1 = \frac{1}{2\tilde{\mathcal{L}}}\int_{-\tilde{\mathcal{L}}}^{\tilde{\mathcal{L}}}(1-\mathcal{C})\mathrm{d}\tilde{\zeta}. \tag{89}$$

For a stable solution, the concentration decreases with height; it is easy to see that for this to be the case, we must have $\tilde{\zeta}_0 \geq \tilde{\mathcal{L}}$, which also guarantees that the concentration is non-negative. Applying (89) to C_0, one finds that $\tilde{\zeta}_0$ is a root of a sixth-order polynomial,

$$\left(\tilde{\zeta}_0 + \tilde{\mathcal{L}}\right)^6 - \left(\tilde{\zeta}_0 - \tilde{\mathcal{L}}\right)^6 = \frac{12\cdot 5^5 \tilde{\mathcal{L}}}{\mathcal{V}^4}. \tag{90}$$

It is straight-forward to show that for a solution $\tilde{\zeta}_0 \geq \tilde{\mathcal{L}}$ to exist, one must require

$$\mathcal{V} \leq \left(\frac{5}{2}\right)^{5/4} 6^{1/4}\tilde{\mathcal{L}}^{-5/4} \equiv \mathcal{V}_{\max}. \tag{91}$$

For any given height of the cell there is thus an upper limit to the applied voltage in order for the term C_0 in the expansion of the concentration to be valid. For solutions where $\mathcal{V} < \mathcal{V}_{\max}$, Eq. 90 must be solved by numerical methods. For the special limiting case where $\mathcal{V} = \mathcal{V}_{\max}$, one finds by analytical means that $\tilde{\zeta}_0 = \tilde{\mathcal{L}}$. It should, however, be pointed out that the resulting solution offers an interpretational challenge at the upper cell boundary, since the concentration gradient vanishes there, which implies infinitely thick vertical boundary layers through (56). This limitation is not very serious, however, as we already know that our solution is only valid outside the boundary layers on the horizontal cell boundaries.

It turns out that $\mathcal{V}_{\max} = 3.8$ for the base case of parameter settings, which is too low for the approximate expression of $\mathcal{C}$ to be accurate. In this case, one has to resort to the reduced evolution equation and transcendental function to compute $\mathcal{C}$; however, an adjustment of the width, h = 0.1 m, of the electrochemical cell for the base case, whilst retaining $\mathcal{H} = 5$, raises the maximal applied voltage to $\mathcal{V}_{\max} = 12.1$, which is depicted in Fig. 9 for the formula (88), and the numerical solution of the steady state of (79) for four different values of $\mathcal{V}$ and for $\mathcal{V} = \mathcal{V}_{\max}$. The semi-analytical expression for $\mathcal{V} < \mathcal{V}_{\max}$ and the closed analytical expression for $\mathcal{V} = \mathcal{V}_{\max}$ can be seen to agree well with the numerically computed steady-state of the evolution Eq. 79.

Proceeding to small values of $\mathcal{V}$, which corresponds to the case of linearized reaction kinetics, an expression for $\Phi_1(\mathcal{C})$ can be secured from regular perturbation theory:

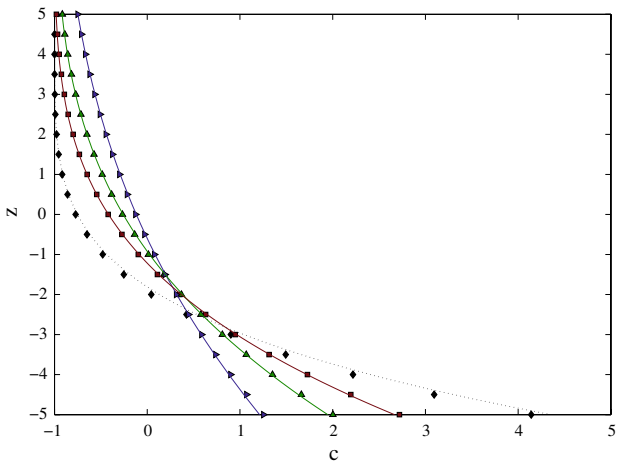

Fig. 9 The vertical steady-state stratification. Comparisons between the solutions (x = 0) for large $\mathcal{V}$ given by (88) (solid curves) and the corresponding numerical steady-state solutions of the evolution Eq. 79, for $\mathcal{V} = 3$ (▷), $\mathcal{V} = 5$ (△) and $\mathcal{V} = 7$ (□). This comparison is also made for the limiting case, where $\mathcal{V} = \mathcal{V}_{\max}$ (◇). Here, Ra = $1.74\cdot 10^5$, $\Gamma = -10.3$, κ = 7.2, and $\mathcal{H} = 5$

$$\Phi_1 = -\frac{1}{1+\sigma(1-\mathcal{C})^{1/2}}\mathcal{V} + \mathcal{O}(\mathcal{V}^3). \tag{92}$$

For physical reasons, it is natural to assume that, in this situation, the concentration $\mathcal{C}$ is also small, whence, from iteration, one finds that

$$\mathcal{C}(\zeta) = \left[\frac{\kappa\sigma}{(1+\sigma)^2}\right]^{2/5}\mathcal{V}^{4/5}\zeta, \tag{93}$$

where the requirement of global conservation of mass has been accounted for. As expected, the stratification is linear in this case. This formula is compared in Fig. 10 with the corresponding steady numerical solution of (79) for small values of the applied voltage $\mathcal{V}$. The agreement is surprisingly good even up to $\mathcal{V} = 0.5$.

The total electric current $\mathcal{I}$ is now defined by

$$\mathcal{I} = \int_{-\mathcal{L}}^{\mathcal{L}} \boldsymbol{i}\cdot\boldsymbol{e}_x|_{x=-1}\mathrm{d}\zeta. \tag{94}$$

From substitution of (83) with the expression for Φ_1 in the present limit (85) together with (88) into (94) one arrives for $\mathcal{V} \gg 1$ at the following expression for the total current (the correction term is given in the appendix):

$$\mathcal{I} \approx 4\sigma\mathcal{L}\mathcal{V}. \tag{95}$$

This expression together with the correction term gives for $\mathcal{V} = \mathcal{V}_{\max}$ the value $\mathcal{I} = 3.3$. This should be compared to the corresponding value calculated from the numerical solution to the steady version of (79) which is $\mathcal{I} = 3.6$.

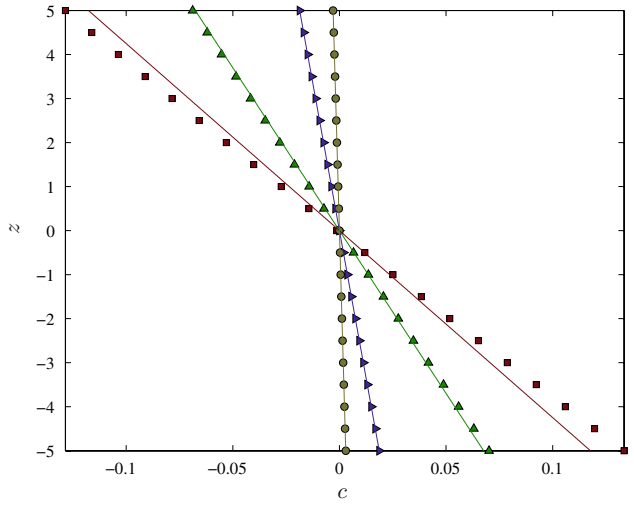

Fig. 10 The vertical steady-state stratification. Comparisons ($x = 0$) between the solutions for small $\mathcal{V}$ given by (93) (solid curves) and the corresponding numerical steady-state solutions of the evolution Eq. 79, for $\mathcal{V} = 0.01$ (○), $\mathcal{V} = 0.1$ (▷), $\mathcal{V} = 0.5$ (△), and $\mathcal{V} = 1$ (□)

Thus the error is $\sim 8\%$, which is acceptable given the fact that $\mathcal{V}_{\max} = 12.1$ is not really large. For $\mathcal{V} > \mathcal{V}_{\max}$, the physical model of the motion of the electrolyte breaks down, c.f. the discussion following (91). Thus, no limiting current was predicted by this simplified theory. The total current for the case of small values of $\mathcal{V}$ is given by

$$\mathcal{I} = \frac{4\sigma}{1+\sigma}\mathcal{L}\mathcal{V} + \mathcal{O}\left(\mathcal{V}^{13/5}\right). \tag{96}$$

This result is illustrated and compared with the numerical solution of (79) for the polarization curve in Fig. 11. The corresponding expression for a free electrolyte found in [3] is erroneous, and should be replaced with:

$$\mathcal{I} = 2^{9/4}\sigma\mathcal{L}\mathcal{V},$$

where the somewhat different notation in [3] has been used.

Clearly, the closed analytical expressions capture the behavior of the overall current density in their respective limits.

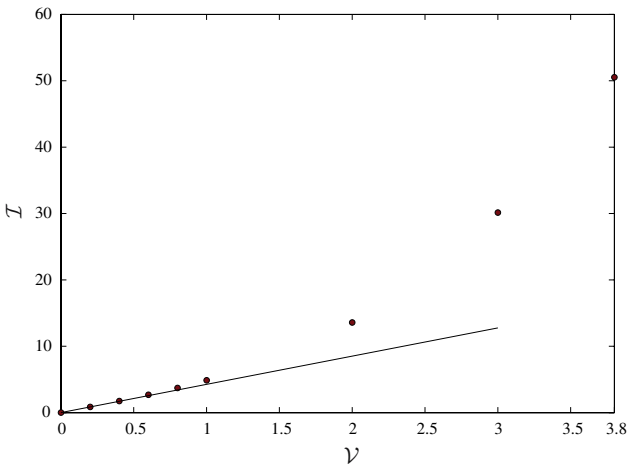

Fig. 11 The polarization curve: comparison between the steady solution of (79), (•), and formula (96) (solid line)

9 Conclusions

Unsteady electrolysis of a binary electrolyte confined to a porous separator has been investigated for large values of Rayleigh number. It has been shown that mass transport takes place mainly in vertical boundary layers at the electrodes with the thickness of the order of $\mathrm{Ra}^{-2/5}$. An evolution equation for the concentration as a function of time and the vertical coordinate, coupled with a transcendental equation, has been derived using perturbation methods. The solution of the simplified equations was then compared with the corresponding numerical solution of the full problem for various situations, and the agreement was found to be good. Further reductions were possible for the case of steady-state conditions and in the limit of small and large cell voltages: for the former, closed analytical solutions were secured for the potential and concentration. For the latter, a semi-analytical expression was derived for the case of $\mathcal{V} < \mathcal{V}_{\max}$, and in the form of a closed analytical expression for the case of $\mathcal{V} = \mathcal{V}_{\max}$. Finally, the overall current could be secured in both limits, i.e., small and large potentials.

Acknowledgments K.B. carried out parts of this work during his stay at Kyoto University as a JSPS-postdoctoral fellow (short term). He would like to thank professor Kazuo Aoki at the Department of Mechanical Engineering and Science, Kyoto University, for encouragement.

10 Appendix

For the correction term C_1 for the concentration, one finds that

$$\begin{aligned}\mathrm{C}_1(\tilde{\zeta}) &= \mathrm{C}_1(-\tilde{\mathcal{L}})\left[\frac{\mathrm{C}_0(\tilde{\zeta})}{\mathrm{C}_0(-\tilde{\mathcal{L}})}\right]^{4/5} + \frac{4}{5\mathcal{V}^{1/5}}\left[\mathrm{C}_0(\tilde{\zeta})\right]^{4/5} \\ &\times \int_{-\tilde{\mathcal{L}}}^{\tilde{\zeta}} \operatorname{arcsinh}\left\{\sigma\mathcal{V}\left[\mathrm{C}_0(\tilde{\zeta}')\right]^{1/2}\right\} \mathrm{d}\tilde{\zeta}'.\end{aligned} \tag{97}$$

The constant $\mathrm{C}_1(-\tilde{\mathcal{L}})$ should be determined so that the sum $\mathrm{C}_0 + \mathrm{C}_1$ satisfies the requirement (89). This yields, after some algebra,

$$C_1(-\mathcal{L}) = \frac{4}{5\mathcal{V}^{1/5}}\left[\frac{C_0^{4/5}(-\mathcal{L})}{C_0(-\mathcal{L}) - C_0(\mathcal{L})}\right] \times \int_{-\mathcal{L}}^{\mathcal{L}} \left[C_0(\mathcal{L}) - C_0(\tilde{\zeta})\right] \operatorname{arcsinh}\left[\sigma\mathcal{V}\sqrt{C_0(\tilde{\zeta})}\right] d\tilde{\zeta}. \quad (98)$$

For the special case $\mathcal{V} = \mathcal{V}_{max}$ one gets

$$C_1(-\tilde{\mathcal{L}}) = -\frac{4}{5 \cdot 6^{1/5}\mathcal{V}_{max}^{1/5}}\mathcal{J}, \quad (99)$$

where the integral $\mathcal{J}$ in the above expression, given by

$$\mathcal{J} = \int_{-\tilde{\mathcal{L}}}^{\tilde{\mathcal{L}}} \mathcal{V}_{max}^4 \frac{(\tilde{\mathcal{L}} - \tilde{\zeta})^5}{5^5} \operatorname{arcsinh}\left[\sigma\mathcal{V}_{max}^3\left(\frac{\tilde{\mathcal{L}} - \tilde{\zeta}}{5}\right)^{5/2}\right] d\tilde{\zeta} \quad (100)$$

can be performed explicitly in terms of elliptic functions. As the applied voltage is assumed to be large, $\mathcal{J}$ can be expanded for large values of $\mathcal{V}_{max}$, and one finds

$$\mathcal{J} = \tilde{\mathcal{L}}\ln(2\sigma\mathcal{V}_{max}) + \ldots \quad (101)$$

and the following expression for the correction term C_1 of the concentration:

$$C_1 = -\frac{4}{15}\mathcal{V}_{max}^3 \frac{(\tilde{\mathcal{L}} - \tilde{\zeta})^4}{5^4}\left\{\tilde{\mathcal{L}}\ln(2\sigma\mathcal{V}_{max}) - 3\int_{-\tilde{\mathcal{L}}}^{\tilde{\zeta}} \operatorname{arcsinh}\left[\sigma\mathcal{V}_{max}^3\left(\frac{\tilde{\mathcal{L}} - \tilde{\zeta}'}{5}\right)^{5/2}\right] d\tilde{\zeta}'\right\}. \quad (102)$$

The correction term for the polarization curve where $\mathcal{V} = \mathcal{V}_{max}$ also contains the integral $\mathcal{J}$, and is given by

$$\mathcal{I}^{(1)} = -4\sigma\mathcal{L}\ln(2\sigma\mathcal{V}_{max}). \quad (103)$$

Further, the correction to the concentration profile when the applied voltage is small is found to be

$$\mathcal{C}^{(1)} = \frac{1}{15}\frac{(2+\sigma)}{(1+\sigma)^{13/5}}\mathcal{V}^{8/5}\left(\tilde{\mathcal{L}}^2 - 3\tilde{\zeta}^2\right). \quad (104)$$

References

1. Karlsson RI, Alavyoon F, Eklund A (1990) In: Proceedings of 3rd International Conference on Laser Anemometry. BHRA/-Springer, pp 329–337
2. Eklund A, Alavyoon F, Simonsson D, Karlsson RI, Bark FH (1991) Electrochim Acta 36:1345
3. Bark FH, Alavyoon F (1995). J Fluid Mech 290:1
4. Wallgren CF, Bark FH, Andersson BJ (1996) Electrochim Acta 41:2909
5. Bark FH (1990) Electrochim Acta 35(2):307
6. Marshall G, Mocskos P, Swinney HL, Huth JM (1999). Phys Rev E 59(2):2157
7. Duchanoy C, Lapicque F, Oduoza CF, Wragg AA (2000) Electrochim Acta 46:433
8. Byrne P, Fontes E, Parhammar O, Lindbergh G (2001) J Electrochem Soc 148(10):125
9. Grigin AP, Davydov AD (1998) Russian J Electrochem 34(11):1237
10. Ruhling K, Winsel A (1989) J Appl Electrochem 19:553
11. Whitaker S (1999) The method of volume averaging. Kluwer Academic Publishers, Dordrecht
12. Kaviany M (1999) Principles of heat transfer in porous media, 2nd edn. Springer-Verlag, New York
13. Newman JS (1991) Electrochemical systems, 2nd edn. Prentice-Hall, New York
14. Bear J, Bachmat Y (1990) Introduction to modeling of transport phenomena in porous media. Kluwer, Dordrecht
15. Comsol Multiphysics, http://www.comsol.com. Accessed 10 May 2006
16. Matlab, http://www.mathworks.com. Accessed 10 May 2006
17. Bark FH, Alavyoon F, Dahlkild AA (1992) J Fluid Mech 235:665
18. Kevorkian J, Cole JD (1981) Perturbation methods in Applied Mathematics. Springer-Verlag Inc, New York